Fuel Processing Technology 209 (2020) 106530

Contents lists available at ScienceDirect

Fuel Processing Technology

journal homepage: www.elsevier.com/locate/fuproc

Research article

# $CO_2$ capture by modified hollow fiber membrane contactor: Numerical study on membrane structure and membrane wettability

Hamed Abdolahi-Mansoorkhani[a], Sadegh Seddighi[a,b,*]

[a] Department of Mechanical Engineering, K. N. Toosi University of Technology, Tehran, Iran
[b] Division of Energy Technology, Chalmers University of Technology, Göteborg, Sweden

ARTICLE INFO

*Keywords:*
$CO_2$ separation
Membrane
Nanoparticles
Carbon capture
Mathematical modeling

ABSTRACT

This work aims at capturing $CO_2$ from natural gas using a verified finite element mathematical model by improving the membrane wettability, membrane structure, the type of absorbents used in the system, and the physical parameters like membrane porosity and the number of fibers used in hollow fiber membrane contactor (HFMC). The model is developed to simulate the $CO_2$ removal using membranes by considering mass transfer equations in the presence of chemical reactions. Simulations were performed using a membrane system including 10 fibers with 175 mm length, 830 μm outer fiber radius and 450 μm inner fiber radius. The effect of adding montmorillonite nanoparticles (MMT) in weight percentages of 1%, 3%, and 5% to the PVDF membrane was perused to demonstrate the influence of membrane structure modification on system performance. The results show that the modification of membrane structure with montmorillonite nanoparticles could increase the efficiency of the system in the removal of $CO_2$ particles by 8%. Four absorbents including MEA (monoethanol amine), PZ (piperazine), TEA (triethanolamine), and EDA (ethylenediamine) are used to identify the most effective absorbent where PZ absorbent shows the highest and EDA absorbent has the lowest carbon capture efficiency. Wettability is found to have a considerably negative impact on membrane carbon capture capacity. For instance, the modeling results show that even a 10% wetting of the membrane reduces the efficiency of the $CO_2$ removal process by more than 47%. In addition, the results illustrate that the increase in membrane tortuosity and gas velocity have negative impacts on the separation process, while increase in the absorbent concentration, packing density and porosity enhance the separation of $CO_2$.

## 1. Introduction

The atmospheric emission of greenhouse gases have increased by 6% annually posing serious threats to the life on earth [1,2]. To address the harmful effects of greenhouse gas emission on the environment, governments, academics and industries are looking for solutions to reduce and prevent the entry of gases such as $CO_2$ into the atmosphere leading to the development of a variety of methods and technologies whose ultimate goal is to reduce $CO_2$ emissions into the atmosphere [3–5].

Renewable energy, electrification, energy efficiency and carbon capture and storage (CCS) are expected to be key elements in decarburization of the energy sector [6,7]. Carbon capture, as the focus of this work, can be pursued using pre-combustion, oxy-fuel combustion or post-combustion capture methods [8,9]. The captured carbon can be either stored in deep saline aquifer [10] or used as a feedstock for carbon dioxide methanation using for instance membranes [11]. Natural gas which has one of the lowest carbon to hydrogen ratios among fossil fuels and consequently is one of the cleanest fossil fuels, contains a share of $CO_2$ mixed with methane ($CH_4$) that is the main ingredient of natural gas [12,13]. To remove and capture unwanted species, various methods such as adsorption and absorption [14–17] and membranes are widely used [18,19].

Membranes have been used for various purposes in recent decades. Some membranes are used to act as a selective boundary controlling the passage of various types of gases. For instance, Pd-Cu/$Al_2O_3$ membrane is used for hydrogen separation, high-performance multi-layer composite membranes are used for $CO_2$ separation and graphene oxide/$TiO_2$-alumina nanocomposite membranes are used for hydrogen separation [20–24]. Easy operation and flexibility in design and construction made membrane technologies rapidly growing for gas separation [25,26].

Among various membrane types, hollow fiber membrane contactors (HFMC) became popular due to their superior performance in various separation technologies [27]. In this system, membrane as a physical

* Corresponding author at: Department of Mechanical Engineering, K. N. Toosi University of Technology, Tehran, Iran.
*E-mail address:* sadeghsk@kth.se (S. Seddighi).

https://doi.org/10.1016/j.fuproc.2020.106530
Received 5 May 2020; Received in revised form 12 July 2020; Accepted 14 July 2020
Available online 23 July 2020
0378-3820/ 

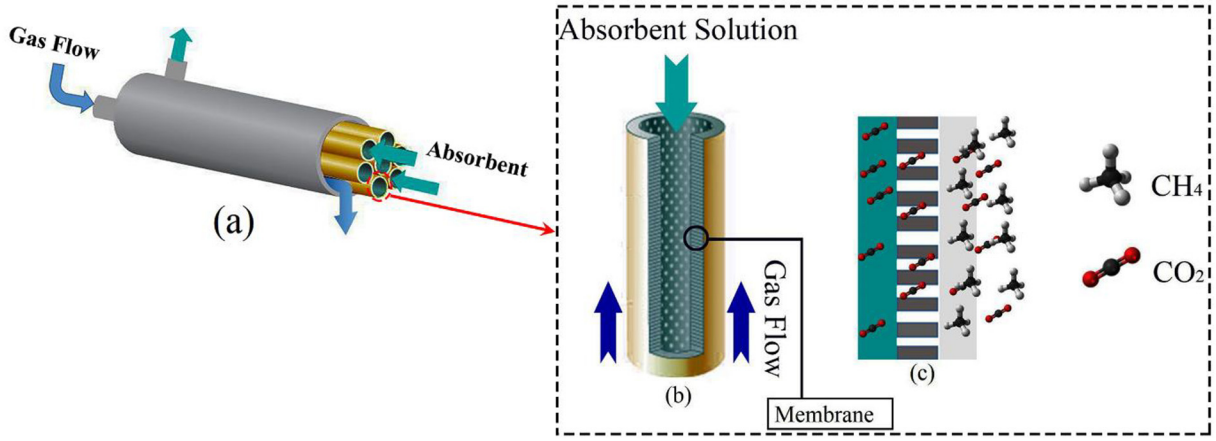


**Fig. 1.** a: 3-D schematic diagram for HFMC module. b: 3-D schematic diagram of a single hollow fiber. c: Schematic diagram of mass transfer of $CO_2$ through membrane.

boundary enables the contact between gas and fluid for mass transfer without direct contact and complete mixing [28,29]. Good mixing is critical in proper operation of any large-scale chemical/reactor system and be thoroughly designed to prevent poorly mixed reactant passage through the reactor [30]. In this system, the desired gas flow passes through the membrane pores to react with the absorbent and subsequently separation process takes place. HFMC systems offer functional physical structure, simple control of the gas and fluid flow rates and high surface contact area per unit area that cause an increase in the efficiency of separation has been used in different applications [29,31]. HFMC consists of three parts as below:

- Shell part which passes the gas stream,
- Membrane that is the porous barrier between gas and absorbents,
- Tube part which contains absorbent flow.

Enhancing the separation efficiency by improving the HFMC membrane structure is one of the topics of interest to researchers [32,33]. The membrane used in the system determines the resistance of the system against heat, pressure and humidity in addition to determining the gas flux. The membrane resistance to wetting is the most vital factor in membrane selection in HFMC structures [34–36]. In general, the membrane used in the structure of HFMC determines the lifetime of the system.

Therefore, researchers have conducted extensive research to improve membrane structures and construct new membranes to increase the efficiency of membrane contact systems. Polypropylene (PP), polyethylene (PE), polytetrafluoroethylene (PTFE), and polyvinylidene fluoride (PVDF) are the most used membrane materials in HFMC [1,36,37]. Hydrophobicity, heat and pressure resistance, as well as the simpler complex structure that reduce the cost of membrane fabrication, are the most important factors in choosing the type of membrane and its material [37–40]. PTFE membranes have better hydrophobicity than membranes such as PP, although the complex structure of PTFE membranes causes a higher production cost for PTFE compared to PP and PVDF [41]. The complex structure and high production cost of membranes such as PTFE have led researchers to pursue other commonly used membrane structures such as PVDF. Addition of nanoparticles to the membranes and the fabrication of composite membranes are among the major membrane modification routes resulting in improved membrane performance [42,43].

Performance of various absorbents used in systems HFMC systems is also of critical importance. The absorption process in the HFMC consists of the transfer of one or more components of the gas phase to the liquid phase that may occur using physical or chemical absorbents. Chemical absorbents have a faster reaction rate and more absorption capacity than physical absorbents, which makes the use of chemical absorbents more favorable than the physical absorbents when looking at economic and efficiency perspectives [44–46]. Due to the important role of the absorbents in the capturing $CO_2$ in HFMC systems, researchers have had extensive research to produce new absorbents in recent years, which in addition to good reactivity with $CO_2$ have high surface tension to minimize the membrane wettability. Besides, the chemical compatibility of absorbents with membrane materials is another key factor contributing to the stability of the membrane systems [44,47,48].

The main objective of this research is to enhance the HFMC separation efficiency by 1) considering the effects of wetting on membrane performance, 2) improve the membrane structure using montmorillonite nanoparticles, and 3) select more efficient absorbents for carbon capture. For this purpose, effects of the addition of montmorillonite nanoparticles to the membrane on HFMC performance were investigated. To investigate the effects of membrane wetting on HFMC performance, the separation performance is analyzed in three cases including the non-wet membrane, the wet membrane, and the partial-wet membrane. The work is based on a mathematical model developed covering both fluid flow and reaction mechanisms involved in $CO_2$ separation.

## 2. Modeling

In order to study the performance $CO_2$ capture from gas mixture using of HFMC a mathematical 2D finite element model of HFMC is developed and used in this work. The mass transfer process was analyzed in three zones consist of shell, tube, and membrane part. The effect of membrane wetting on system capability to remove $CO_2$ particles was studied in three cases of wet membrane, partial-wet membrane, and non-wet membrane. The membrane used in the system is based on the PVDF structure. In order to investigate the effect of modifying the membrane structure on system performance, the effect of the presence of different weight percentages of montmorillonite nanoparticles (MMT) on the system structure was evaluated. This work also compares the performance of the system when changing the chemical absorbent between four chemical absorbents of PZ, TEA, MEA, and EDA.

In Fig. 1a, the overall 3D schematic of the separating system (HFMC) is shown. In this HFMC structure, absorbent flows in the hollow. The gas mixture is passing from the shell side. As shown Fig. 1b and c, the gas mixture is flowing around the single hollow fiber and the absorbent is entering the pipe in the opposite direction to the gas mixture. The membrane is taking the role of the separating boundary. Schematic of model domain development for porous HFMC under non-wetting of operation is depicted in Fig. 2. The physical parameters and

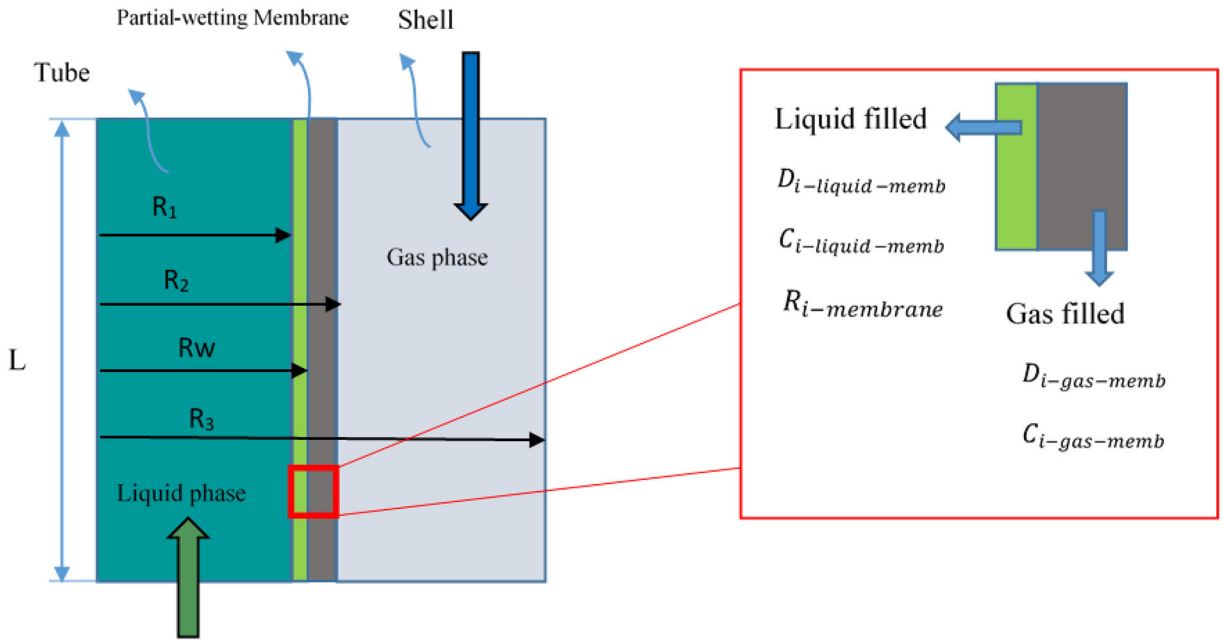


**Fig. 2.** A 2-D the schematic of the membrane contactor considering membrane wetting.

**Table 1**
The properties of the modeled membrane contactor module according to [49].

| The membrane parameter | Value |
|---|---|
| Module length (mm) | 250 |
| Fiber O.D. (μm) | 830 |
| Fiber I.D. (μm) | 450 |
| Number of fibers | 10 |
| Effective fiber length (mm) | 175 |

**Table 2**
The physical properties of the modeled membrane according to [49].

| %MMT/ PVDF | Mean pore size (μm) | Effective surface porosity ($m^{-1}$) | Water contact angle (°) |
|---|---|---|---|
| 0% | 26 | 87 | 80 |
| 1% | 32 | 124 | 84 |
| 3% | 34 | 171 | 88 |
| 5% | 22 | 237 | 99 |

model geometry dimension of simulated system are given in Tables 1 and 2.

The gas mixture includes 90% methane and 10% $CO_2$. The process is steady-state while no reaction takes place in the shell side. The gas flow is assumed to follow the ideal gas law while flows are assumed to be laminar. Pore size in whole of membrane was considered equal and uniform. Isothermal condition was applied within the shell and tube side. Henry's law was applied to gas-liquid equilibrium.

The steady-state continuity equation for each species with considering chemical reaction can be expressed as [50]:

$$\frac{\partial C_i}{\partial t} = -\nabla \bullet J_i + R_i \tag{1}$$

where $J_i$ is flux, $C_i$ is concentration, and $R_i$ is the rate of reaction each for specie $i$. The flux is calculated according to Fick's law [51]:

$$J_i = -D_i \nabla C_i + C_i V_z \tag{2}$$

where $D_i$ is the diffusivity of specie $i$ and $V_z$ is the velocity in the direction of the module. Based on Eqs. (1) and (2), the general mass balance equation is found as below:

$$\frac{\partial C_i}{\partial t} = -\nabla \bullet (-D_i \nabla C_i + C_i V_z) + R_i \tag{3}$$

### 2.1. Shell side modeling

The continuity equation for $CO_2$ in shell side written as below where $R_i$ is removed since there is no reaction in the shell side:

$$D_{CO_2-shell}\left[\frac{\partial^2 C_{CO_2-shell}}{\partial r^2} + \frac{1}{r}\frac{\partial C_{CO_2-shell}}{\partial r} + \frac{\partial^2 C_{CO_2-shell}}{\partial z^2}\right] = V_{z-shell}\frac{\partial C_{CO_2-shell}}{\partial z} \tag{4}$$

Happel's free surface model is applied to calculate the velocity distribution in hollow fibers. Fig. 3 depicts the cross-sectional zone of the hollow fiber membrane contractor. According to Happel's free surface model [52], only a division of fluid encompassing the fiber is considered and could be approximated as a circular cross-section.

The laminar parabolic velocity profile outside the hollow fiber is given as below [52]:

$$V_{z-shell} = 2u\left[1 - \left(\frac{R_2}{R_3}\right)^2\right] \times \left[\frac{\left(\frac{r}{R^3}\right)^2 - \left(\frac{R_2}{R_3}\right)^2 + 2\ln\left(\frac{R_2}{r}\right)^2}{3 + \left(\frac{R_2}{R_3}\right)^4 - 4\left(\frac{R_2}{R_3}\right)^2 + 4\ln\left(\frac{R_2}{R_3}\right)}\right] \tag{5}$$

where u is the average velocity in shell side, R3 is the radius of free surface, $R_2$ is the outer radius of fibers (see Fig. 2). The radius of free surface can be calculated as below:

$$R_3 = R_2\sqrt{1/(1-\varphi)} \tag{6}$$

where $\varphi$ is the volume fraction of the void inside the membrane contactor Which follows from the following equation:

$$1 - \varphi = \frac{nR_2^2}{\mathbb{R}^2} \tag{7}$$

where n is the number of fibers and $\mathbb{R}$ is the module inner radius.

Boundary conditions in the shell side are given as below.

$$z = L \qquad C_{i-shell} = C_{initial} \qquad i = CO_2 \tag{8}$$

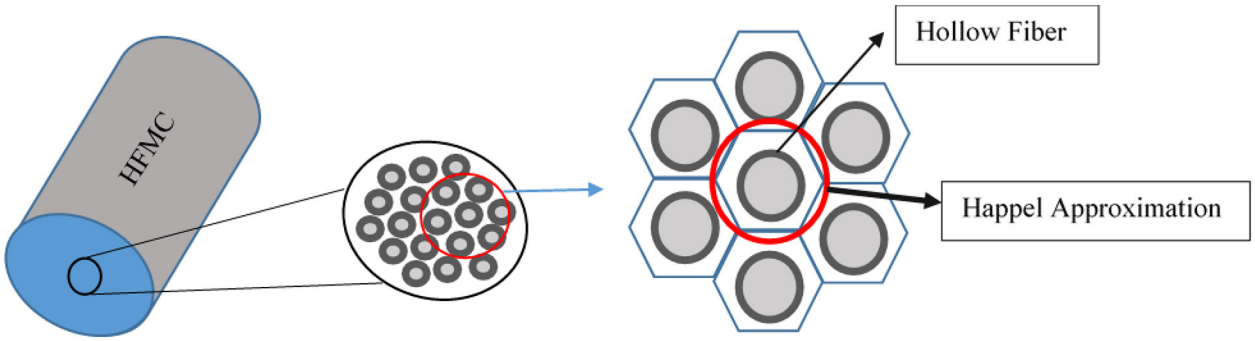


**Fig. 3.** Hypothetical circle-shaped approximation and cross sectional based on Happel approximation.

$$r = R_2 \qquad C_{i-shell} = C_{i-membrane} \tag{9}$$

$$r = R_3 \qquad \frac{\partial C_{i-shell}}{\partial r} = 0 \tag{10}$$

### 2.2. Membrane side equations (non-wetting)

Assuming the pores are filled with gas, inside the membrane can be assumed to have only one phase that is gas. Thus, the steady state continuity equation for $CO_2$ in membrane can be written according to the dispersion as below:

$$D_{i-membrane}\left[\frac{\partial^2 C_{i-membrane}}{\partial r^2} + \frac{1}{r}\frac{\partial C_{i-membrane}}{\partial r} + \frac{\partial^2 C_{i-membrane}}{\partial z^2}\right] = 0 \tag{11}$$

where $D_{i\text{-}membrane}$ is the diffusivity coefficient of $CO_2$ in the membrane which is dependent on the porosity and tortuosity.

For i = $CO_2$

$$D_{CO_2-membrane}\ (\mathrm{m^2\ S^{-1}}) = D_{CO_2-shell}(\varepsilon/\tau) \tag{12}$$

The boundary conditions for solving the membrane equation are given below:

$$C_{i-membrane} = \frac{C_{i-Tube}}{m_i}\ at\ r = R_1 \tag{13}$$

where $m_i$ is solubility of $CO_2$ in absorbent that achieved from Henry's law.

$$C_{i-shell} = C_{i-membrane}\ at\ r = R_2 \tag{14}$$

### 2.3. Membrane side equations including wetting

In membrane systems where there is a constant contact surface between the porous membrane and the absorbent, part of the membrane (Fig. 2) is wetted by the absorbent due to the interaction between the surface and the absorbent and subsequently by a decrease in surface tension. It is, therefore, necessary to rewrite the membrane-governing equations for two parts, 1: the gas-filled membrane area and 2: the absorbent-filled area.

Part filled with gas:

As shown in Fig. 2, the right side of the membrane is filled with gas. Hence, the phenomenon of diffusion within the membrane can be written only on the basis of the diffusion of $CO_2$ gas particles as follows:

$$D_{i-gas-membrane}\left[\frac{\partial^2 C_{i--gas-membrane}}{\partial r^2} + \frac{1}{r}\frac{\partial C_{i-gas-membrane}}{\partial r} + \frac{\partial^2 C_{i-gas-membrane}}{\partial z^2}\right] = 0 \tag{15}$$

The boundary condition is given as:

$$C_{i-gas-membrane} = \frac{C_{i-liquid-membrane}}{m_i} \qquad at\ r = R_w \tag{16}$$

where $m_i$ is solubility of $CO_2$ in absorbent that achieved from Henry's law.

$$C_{i-shell} = C_{i-gas-membrane} \qquad at\ r = R_2 \tag{17}$$

Part filled with absorbent:

As shown in Fig. 2, the left side of the membrane is filled with absorbent. Hence, the phenomenon of diffusion within this part of the membrane can be written on the basis of the diffusion of $CO_2$ gas molecules from gas side toward the absorbents and reaction between $CO_2$ molecules and absorbent as follows [34]:

$$D_{i-liquid-membrane}\left[\frac{\partial^2 C_{i-liquid-membrane}}{\partial r^2} + \frac{1}{r}\frac{\partial C_{i-liquid-membrane}}{\partial r} + \frac{\partial^2 C_{i-liquid-membrane}}{\partial z^2}\right] + R_{i-membrane} = 0 \tag{18}$$

The boundary conditions are given as:

$$C_{i-gas-membrane} = C_{i-liquid-membrane} \times m\_i \qquad at\ r = R_w \tag{19}$$

where $m_i$ is solubility of $CO_2$ in absorbent that achieved from Henry's law.

$$C_{i-tube} = C_{i-liquid-membrane} \qquad at\ r = R_1 \tag{20}$$

Proceeding with the reaction depends the porosity of the membrane and the simultaneous presence of absorbent and gas in the membrane pores. Parameter $R_{i-membrane}$ in Eq. (18) shows the effect of the reaction performed on the transport phenomenon in the wet part of the membrane that is defined as follows [53]:

$$R_{i-membrane} = R_i \times \varepsilon \tag{21}$$

### 2.4. Tube side equations

The steady state continuity equation for transport of $CO_2$ while reacting with absorbents in the tube changing the specie composition is given below where convection, dispersion (using Fick's law) and reaction are included.

$$D_{i-tube}\left[\frac{\partial^2 C_{i-tube}}{\partial r^2} + \frac{1}{r}\frac{\partial C_{i-tube}}{\partial r} + \frac{\partial^2 C_{i-tube}}{\partial z^2}\right] + R_i = V_{z-tube}\frac{\partial C_{i-tube}}{\partial z} \tag{22}$$

where $C_i$ is the concentration, $D_i$ is diffusion coefficient and $R_i$ is the reaction term.

Only axial convective mass transfer is assumed since the radial convection is small compared to the axial convection [54]. The velocity distribution is assumed to follow laminar velocity profile as below [55]:

$$V_{z-tube} = 2v\left[1 - \left(\frac{r}{R_1}\right)^2\right] \tag{23}$$

where $v$ is average velocity in tube side. Boundary conditions on tube side are given as below:

$$at\ z = 0, \quad C_{i-tube} = 0, \quad C_{Absorbents-tube} = C_{initial} \quad (i = all\ species) \tag{24}$$

$$at \quad r = 0, \quad \frac{\partial C_{i-tube}}{\partial r} = 0\ (symmetry) \quad (i = all\ species) \tag{25}$$

$$r = R_1, \quad C_{i-tube} = C_{i-membrane} \times m_i \quad (i = CO_2) \tag{26}$$

Diffusion of $CO_2$ in different Absorbents is found according [56] to as below:

$$(D_{CO_2})_{Absorbent} = D_{N_2O,Absorbent}\left(\frac{D_{CO_2,H_2O}}{D_{N_2O,H_2O}}\right) \tag{27}$$

Diffusivity of $CO_2$ and $N_2O$ in water is found as below [56]:

$$(D_{CO_2})_{water} = 2.35 \times 10^{-6}\ \exp\left(-\frac{2119}{T}\right) \tag{28}$$

$$(D_{N_2O})_{water} = 2.35 \times 10^{-6}\ \exp\left(-\frac{2371}{T}\right) \tag{29}$$

The Henri coefficient, which is an important factor in gas stripping, is found as below [56]:

$$(H_{CO_2})_{Absorbent} = H_{N_2O,Absorbent}\left(\frac{H_{CO_2,H_2O}}{H_{N_2O,H_2O}}\right) \tag{30}$$

The parameters of Eq. (29) are found as below [56,57]:

$$H_{CO_2,H_2O} = 2.82 \times 10^6 \exp\left(\frac{2044}{T}\right) \tag{31}$$

$$H_{N_2O,H_2O} = 8.55 \times 10^6 \exp\left(\frac{2284}{T}\right) \tag{32}$$

Reaction kinetics:

The reaction rate of $CO_2$ molecules with absorbents including EDA, PZ, MEA, and TEA and also the molecular structures of the above mentioned absorbents are accounted in Table 3. Chemical properties of $CO_2$, EDA, PZ, MEA and TEA utilized with the purpose of developing comprehensive mathematical modeling are listed in Tables 4 and 5.

It should be noted that the addition of nanoparticles to the membrane is considered in modeling by modifications in membrane properties such membrane porosity and membrane permeability. For instance, the changes relating to the diffusion of carbon dioxide into the membrane are modified when MMT is added using Eqs. (11) and (12) considering modified membrane porosity and tortuosity.

**Table 3**
The reaction rate of $CO_2$ with various absorbents in the tube side of HFMC (temperatures in Kelvin).

| Parameter | Reaction rate (mol/m$^3$ · s) | Reference |
|---|---|---|
| EDA [$C_2H_8N_2$] | $-8.7 \times 10^9 \exp\left(-\frac{6080}{T}\right) C_{CO_2} C_{EDA}$ | [58] |
| PZ [$C_4H_{10}N_2$] | $-4.49 \times 10^{12} \exp\left(-\frac{5712}{T}\right) C_{CO_2} C_{PZ}$ | [59] |
| MEA [$C_2H_7NO$] | $-\left(10^{10.99-\frac{2152}{T}}\right) 10^{-3} C_{CO_2} C_{MEA}$ | [60] |
| TEA [$C_6H_{15}NO_3$] | $-4.52 \times 10^4 \left(\exp\left(-\frac{2688}{T}\right) C_{CO_2} C_{TEA}\right)$ | [61] |

**Table 4**
The properties of the absorbents used in this work.

| Absorbent | MEA | PZ | TEA | EDA |
|---|---|---|---|---|
| Molar Weight (g · mol$^{-1}$) | 61.08 [62] | 86.13 [63] | 149.19 [64] | 60.1 [64] |
| Density (at 298 K) (g · cm$^{-3}$) | 1.01 [62] | 1.1 [63] | 1.12 [65] | 0.89 [66] |
| Boiling point (K) | 443 [62] | 416 [67] | 608 [64] | 391 [64] |
| Flash point (K) | 366 [62] | 360 [67] | 458 [64] | 377 [64] |
| Surface tension (at 298 K) (g · s$^{-2}$) | 48.89 [68] | 70.2 [63] | 48.9 [69] | 36.9 [70] |

**Table 5**
The chemical properties of parameters used in modeling.

| Parameter | Value | Reference |
|---|---|---|
| $D_{CO_2-shell}$ (m$^2$ S$^{-1}$) | $1.8 \times 10^{-5}$ | [71] |
| $D_{CO_2-membrane}$ (m$^2$ S$^{-1}$) | $D_{CO_2-shell}(\varepsilon/\tau)$ | [53] |
| $D_{MEA-tube}$ (m$^2$ S$^{-1}$) | $9.3 \times 10^{-10}$ | [72] |
| $D_{CO2-MEA}$ (m$^2$ S$^{-1}$) | $1.51 \times 10^{-9}$ | [72] |
| $D_{TEA-tube}$ (m$^2$ S$^{-1}$) | $7.11 \times 10^{-10}$ | [73] |
| $D_{CO2-TEA}$ (m$^2$ S$^{-1}$) | $1.95 \times 10^{-9}$ | [73] |
| $D_{PZ-tube}$ (m$^2$ S$^{-1}$) | $1.05 \times 10^{-9}$ | [74] |
| $D_{CO2-PZ}$ (m$^2$ S$^{-1}$) | $1.51 \times 10^{-9}$ | [74] |
| $D_{EDA-tube}$ (m$^2$ S$^{-1}$) | $1.05 \times 10^{-9}$ | [58] |
| $D_{CO2-EDA}$ (m$^2$ S$^{-1}$) | $2.09 \times 10^{-9}$ | [58] |
| $m_{CO_2-MEA}$ (mol · mol$^{-1}$) | 0.81 | [72] |
| $m_{CO_2-EDA}$ (mol · mol$^{-1}$) | 0.4 | [75] |
| $m_{CO_2-PZ}$ (mol · mol$^{-1}$) | 1.06 | [59] |
| $m_{CO_2-TEA}$ (mol · mol$^{-1}$) | 0.6 | [73] |

## 3. Validation and mesh independence

To ensure that the size of the modeling network cells does not affect the results, the grid independence and the stability of the results in different mesh networks are investigated. In this study, the removal of $CO_2$ is investigated in a system with the number of cells from 47,800 to 327,600 cells. According to the results shown in figure below, a grid with 220,000 cells is selected (Fig. 4).

To verify the model, both flux passing through membrane and $CO_2$ concentration are compared to experimental results. Firstly, the fluid

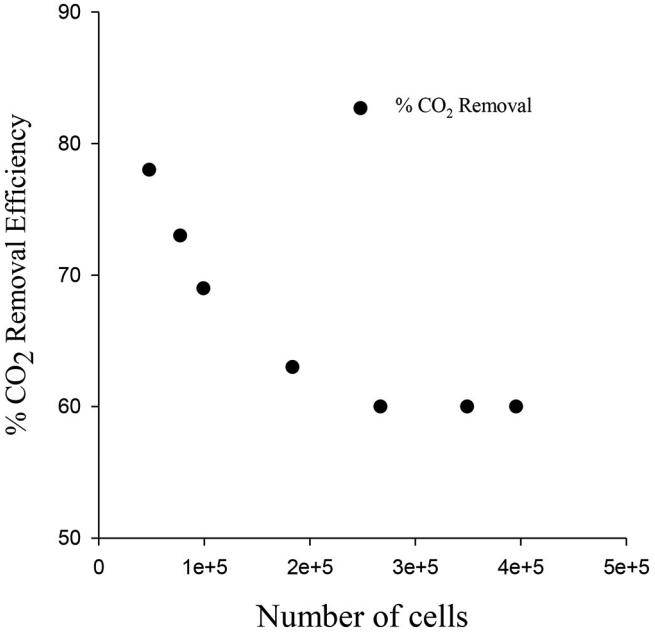


**Fig. 4.** The grid independence using $CO_2$ removal for various number of cells (PVDF membrane, $C_{MEA}$ = 1000 mol m$^{-3}$, $V_{liquid}$ = 1 m/s, $V_{gas}$ = 10 m/s).

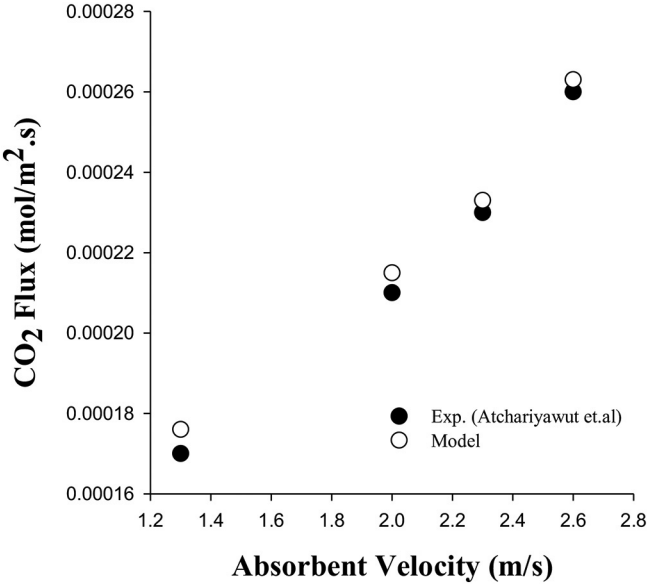


**Fig. 5.** Comparison between the modeled flux of $CO_2$ absorption and the experimental data of Atchariyawut et al. [76] (PVDF, $CO_2 : CH_4 = 20 : 80$, $Gas_T = 30^{\circ}$, gas flow rate: 200 ml · $min^{-1}$).

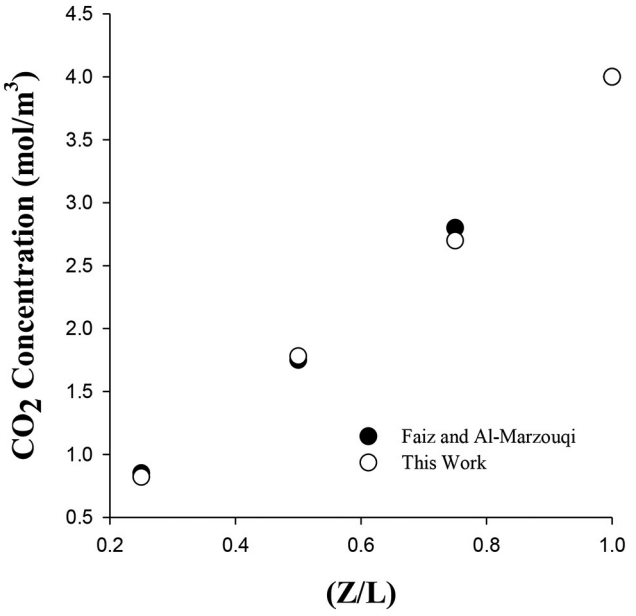


**Fig. 6.** Comparison between the modeled $CO_2$ concentration along the shell and the results reported by Faiz and Al-Marzuqi [53] ($V_{gas} = 3.3$ m/s, $V_{MEA} = 0.67$ m/s, $C_{MEA} = 3000$ mol · $m^{-3}$, gas feed: $C_{CO2}\ inlet = 4$ mol · $m^{-3}$).

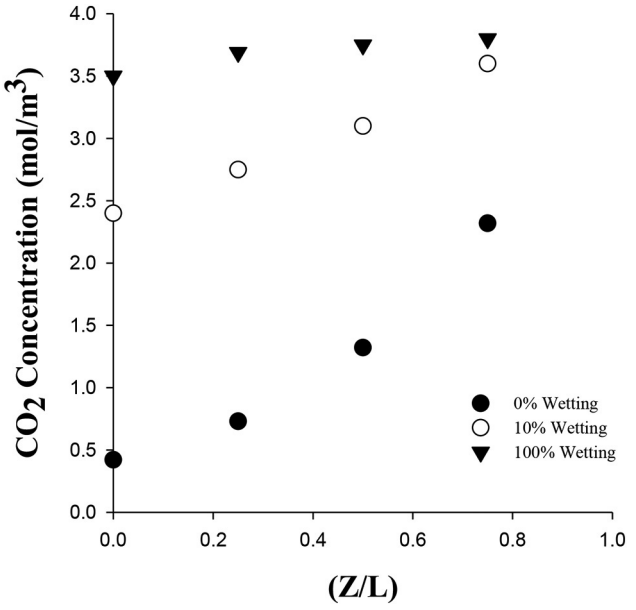


**Fig. 7.** Effect of membrane wettability on $CO_2$ concentration along the membrane length (PVDF, $C_{PZ} = 1000$ mol · $m^{-3}$, $C_{CO2}\ inlet = 4$ mol · $m^{-3}$, $v_{gas} = 5$ m/s, $v_{Abs} = 0.5$ m/s).

mechanics of the modeling is validated. The flux through the membrane compared to the experimental work [76], where the flux passing through the membrane was analyzed in the presence of water as an absorbent. Thereafter, the chemical part validation is performed by comparing the variation of $CO_2$ concentrations inside the system's shell with results given in [53].

The rate of mass transfer is found as below [77].

$$J_{CO2} = (Q_{in} \times C_{in} - Q_{out} \times C_{out}) \times 273.15 \times \frac{1000}{22.4 \times T_g \times S} \quad (33)$$

where $J_{CO2}$ is the $CO_2$ mass transfer rate, $Q_{in}$ and $Q_{out}$ are incoming and outgoing gas flowrates respectively, $C_{in}$ and $C_{out}$ are incoming and outgoing $CO_2$ volume concentration respectively, $T_g$ is the gas temperature and $S$ is the contact surface between gas and liquid.

Fig. 5 shows the modeling comparison with the experimental work [76]. The results show that the outcomes of the modeling of flux variation across the membrane have acceptable conformity with the experimental results. The results show that with increasing the absorption rate of the tube, the amount of $CO_2$ passing through the membrane increases since as the fluid velocity increases in the tube, the thickness of the boundary layer of the fluid near the surface of the membrane decreases leading to a reduced resistance to the penetration of $CO_2$ molecules.

Fig. 6 shows the comparison between the modeled $CO_2$ Concentration along the shell and the results reported by Faiz and Al-Marzuqi [53] showing a good agreement. The results show that when the natural gas flows in the shell side, the diffusion of $CO_2$ molecules inside the membrane reduces the $CO_2$ concentration until reaching the minimum concentration at the end of the shell.

## 4. Results and discussion

Fig. 7 shows the effect of membrane wettability on the performance of the membrane contactor system in three states of wetting, partial wetting, and non-wetting membrane. The results show that the amount of $CO_2$ removal in the non-wetting state of the membrane is higher than those of wetting cases. As seen, the amount of $CO_2$ captured from the system by utilizing the non-wetting membrane case is 0.45 mol · $m^{-3}$ that represents the removal of 87% of the incoming $CO_2$ in the non-wetting membrane. But when adding only 10% wetting to the membrane, the flux of outgoing $CO_2$ gets as high as 2.4 mol · $m^{-3}$ showing 47% less carbon capture by adding only 10% wetting to the membrane properties compared to the non-wetting case. The reason for this difference is that when the pores of the membrane are only filled with gas, due to less penetration resistance than the state where part of the pores of the membrane is filled with absorbent, more flux of $CO_2$ passes through the membrane, which leads to further removal of $CO_2$ from a gas mixture. Therefore, it is necessary to utilize a membrane, which in addition to passing $CO_2$ through membrane pores, has excellent resistance to the penetration of the absorbent in order to enhance the efficiency of the system. The use of multi-layer membranes such addition of absorbent-resistant layer absorbent side, or the use of nanoparticle-modified composite membrane structures, can be

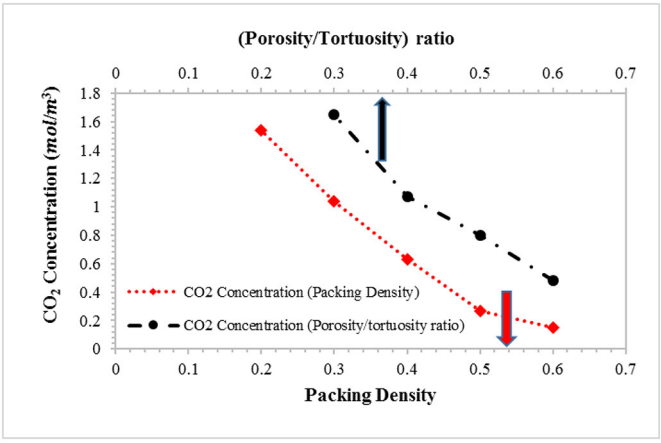


**Fig. 8.** Effect of porosity/tortuosity ratio and Packing density on $CO_2$ outlet concentration ($PZ_{Absorbent}$ = 1000 mol•m$^{-3}$, $v_{gas} = 10\frac{m}{s}$, $v_{Absorbent}$ = 0.5 m/s).

considered as a way to increase system efficiency by improving wettability.

Fig. 8 shows the effect of membrane structure factor (porosity-to-tortuosity ratio or f = ε / τ) in membrane structure on the removal of $CO_2$. When studying fluid flow through a porous media, several major physical phenomena must be investigated including: 1) solid-fluid interactions, 2) reduction in the volume available for fluid flow due to the solid obstacles and 3) longer particle path to cross the tortuous solid structure. Such physical phenomena are modeled using the porosity (ε) and the tortuosity (τ) parameters and by rescaling the transport coefficients according to [78] as below.

$$D = D_{void}(\varepsilon/\tau) \tag{34}$$

where $D_{void}$ is the corresponding parameter in the void space, ε is the fraction of free volume and τ is ratio of the direct distance between two points and the actual distance flow undergoes inside the porous structure. The ratio f = ε / τ is called as the structure factor. This figure confirms that the percentage of $CO_2$ removal significantly increases with the increase in membrane porosity to tortuosity. The relationship between the effective diffusivity of $CO_2$ in the membrane and membrane structure was explained by Eq. (12) which suggests the effective diffusion coefficient of $CO_2$ in the membrane is a function of membrane porosity and membrane tortuosity. By increasing the ratio of these two parameters, the diffusion coefficient increases and consequently the rate of mass transfer of $CO_2$ is increased via the membrane. As a result, $CO_2$ concentration is reduced at the output, leading to an improvement in carbon capture efficiency of the HFMC. In addition, the effect of packing density on the output concentration of $CO_2$from the shell is shown in Fig. 8. As shown, increasing the packing density leads to the reduction in the $CO_2$ output concentration. Eq. (7) shows that the value of the parameter φ is directly proportional to the number of fiber used in the modulus. Increasing the number of fibers used inside the module increases the mass transfer level between the gas phase and the liquid absorbent. As a result, the level of liquid/gas contact increases significantly, which results in improvements in carbon capture from the $CO_2/CH_4$ gas mixture, thereby reducing the $CO_2$ emissions from the shell.

Fig. 9 shows the $CO_2$ flux through the membrane for including non-wetting membrane, partial wetting membrane, and modified membrane. The results show that as the absorbent velocity increases, the flux of $CO_2$ from the membrane increases which is due to the decrease in the thickness of the absorbent boundary layer adjacent to the membrane surface leading to reduction of the resistance of the boundary layer resulting in better penetration of $CO_2$. Besides, increasing the absorbent velocity inside the tube increases the rate of replacement of the spent absorbent by fresh absorbent leading to

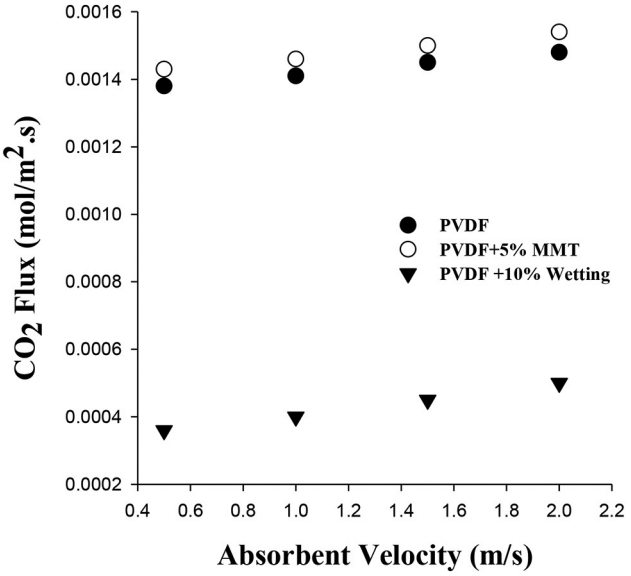


**Fig. 9.** Effect of membrane structure on $CO_2$ flux through the membrane ($v_{gas}$ = 5 m/s, $C_{PZ}$ = 750 mol · m$^{-3}$).

enhanced $CO_2$ capture capacities. It should be noted that increasing the absorbent velocity beyond a certain limit would have little impact on $CO_2$ flux through the membrane because the high absorbent velocity does now give the required residence time for $CO_2$ flux through the membrane. The value found in this work is the absorbent velocity of 2 m/s as the upper limit for absorbent velocity where further absorbent velocities have very small impacts on the dissolution rate of $CO_2$ in the absorbents due to very limited contact time between the absorbent and the membrane. Also, Fig. 9 shows that using a modified membrane (PVDF with 5% wt MMT) leads to higher $CO_2$ fluxes compared to non-wetting membrane (PVDF with 0% wt MMT) and partially wetting membrane due to the modification of the surface physical properties including increased surface porosity and contact angle. These results show the necessity of utilization of a membrane with high permeability and high resistance to wetting.

Fig. 10 shows the effects of MMT nanoparticles addition into the polymer matrix in different loadings (1, 3, 5 wt% of membrane polymer) on the removal of $CO_2$ molecules from the gas mixture. The results show that increasing MMT nanoparticles concentration from 1 to 5 wt% of the membrane leads to 10% more $CO_2$ removal from the system. The main reason for the enhanced carbon capture efficiency in the high MMT nanoparticle concentrations is the modification of the membrane structure: by increasing the weight percent of MMT nanoparticles to the membrane from 0 wt% to 5 wt%, the surface porosity has been increased from 87 m$^{-1}$ in the PVDF (0 wt% MMT) membrane to 237 m$^{-1}$ in the PVDF (+5 wt% MMT), which leads to higher amount of $CO_2$ passing through the membrane compared to the cases with no MMT nanoparticles. In addition, increasing the contact angle between the absorbent and the membrane surface from 88° in PVDF with 0 wt% MMT to 99° in PVDF with +5 wt% MMT, and also reducing the size of the membrane cavities in the PVDF with 5 wt% MMT membrane relative to the PVDF with 0 wt% MMT allow better penetration of $CO_2$ from the shell side to the membrane and consequently to the absorbent channel.

Fig. 11 shows the outgoing $CO_2$ concentration at varying PZ, MEA, TEA, and EDA absorbents concentrations. As shown, by increasing the input absorbents' concentration from 500 mol · m$^{-3}$ to 2000 mol · m$^{-3}$, the outgoing $CO_2$ concentration decreases. The reaction kinetics between the absorbents and $CO_2$ has a direct correlation with the input absorbents' concentration. As the absorbents' concentration increases, there is a higher probability of contact between $CO_2$ and the absorbent

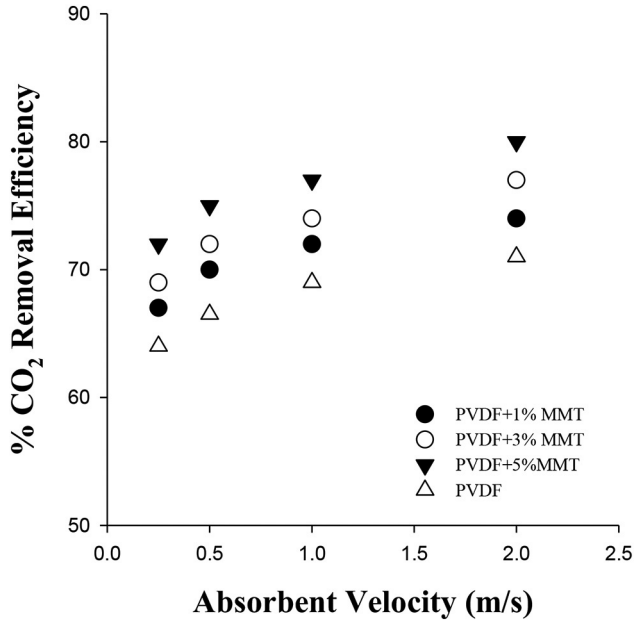


**Fig. 10.** Effect of mass fraction of MMT on removal efficiency of $CO_2$ ($C_{PZ}$ = 750 mol · m$^{-3}$, $v_{gas}$ = 10 m/s).

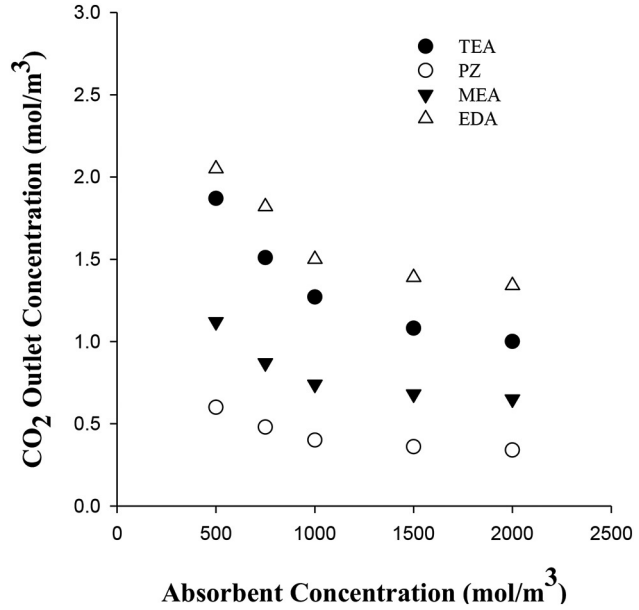


**Fig. 11.** Effect of absorbents mass concentration on $CO_2$ outlet concentration (PVDF, $V_{gas}$ = 5 m/s, $V_{Absorbents}$ = 0.5 m/s, gas feed: $CO_2$ *inlet* = 4 mol · m$^{-3}$, $CH_4$ *inlet* = 36 mol · m$^{-3}$).

leading to improved reaction between the absorbent and the $CO_2$. Thus, higher absorbent concentration causes a higher carbon capture in the vicinity of membrane boundary layers in the tube side. Fig. 11 also shows that the variations in absorbent concentration from 500 to 1500 mol · m$^{-3}$ have higher impact on carbon capture efficiency compared to other absorbent concentrations. Increases in absorbent concentrations above 1500 mol · m$^{-3}$ have little impact on carbon capture efficiency since the absorbents and gas system have reached a saturation state, and the increase in the concentration of the absorbents have no effect on the dissolution rate of $CO_2$ in the absorbents. Fig. 11 also shows that PZ absorbent has a better ability to remove $CO_2$ molecules than other absorbents since PZ molecules have two -NH- groups that directly prepare higher $CO_2$ absorption capacity compared to those of other

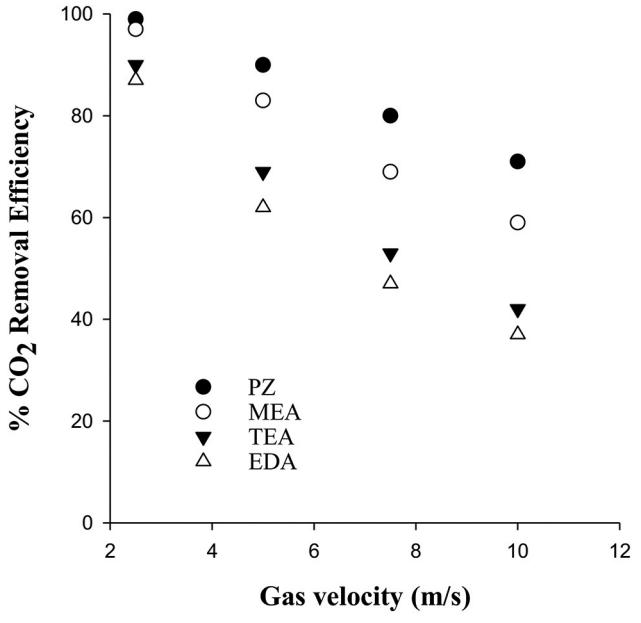


**Fig. 12.** Effect of gas velocity on $CO_2$ removal efficiency (PVDF, $V_{Absorbents}$ = 0.5 m/s, gas feed: $CO_2$ *inlet* = 4 mol · m$^{-3}$, $CH_4$ *inlet* = 36 mol · m$^{-3}$, $C_{inlet}$ *Absorbents* = 1000 mol · m$^{-3}$).

primary/secondary amines with one -$NH_2$/-NH-group.

Fig. 12 shows the carbon capture performance of the HFMC at varying gas velocity at constant absorbent concentration for all absorbents. With increasing the gas velocity, the residence time of $CO_2$ molecules near the membrane's surface is reduced leading to a reduced reaction between the gas and the absorbents' flow. Consequently, $CO_2$ concentration increases in the output of this membrane and the carbon capture efficiency reduces which is in line with findings of [79–81]. It should be noted that in industrial systems, the range of changes in gas flow velocity should be so that the gas flow rate surge does not cause an undesirable decrease in the membrane stage-cut value. For this reason, the gas flow rate should be optimized for economical separation [82,83].

Fig. 13 shows the absorbent consumption at various absorbent velocities. The amount of absorbent consumed in the membrane system depends on the residence time of the absorbent in the tube and the reactivity of absorbent with the passing $CO_2$. As shown, increasing absorbent velocity would lead to reduced absorbent consumption that is due to the reduced absorbent residence time at increased velocities. For instance, increasing absorbent velocity from 0.25 m/s to 2 m/s is associated with 40% reduction in absorbent consumption while $CO_2$ removal increased by 8%. However when absorbent velocity increased from 2 m/s to 3.5 m/s, the 5.5% absorbent consumption reduction is associated with only 1% increase in $CO_2$ removal. Thus, the absorbent velocity of 2 m/s is a saturation limit for absorbent velocity where further increased absorbent velocity have little impact on $CO_2$ removal through the membrane because the high absorbent velocity does now give the required residence time for $CO_2$ flux through the membrane confirming the findings of Fig. 9.

## 5. Conclusion

A modified hollow fiber membrane contactor (HFMC) is used to capture $CO_2$ from a natural gas mixture, including $CO_2$ and $CH_4$ using a verified mathematical model. Modeling different parts of the membrane including shell, membrane, and tube gives the following results:

1. The study performance of different absorbents, PZ, MEA, EDA, and TEA, shows that PZ absorbent has the highest capture performance

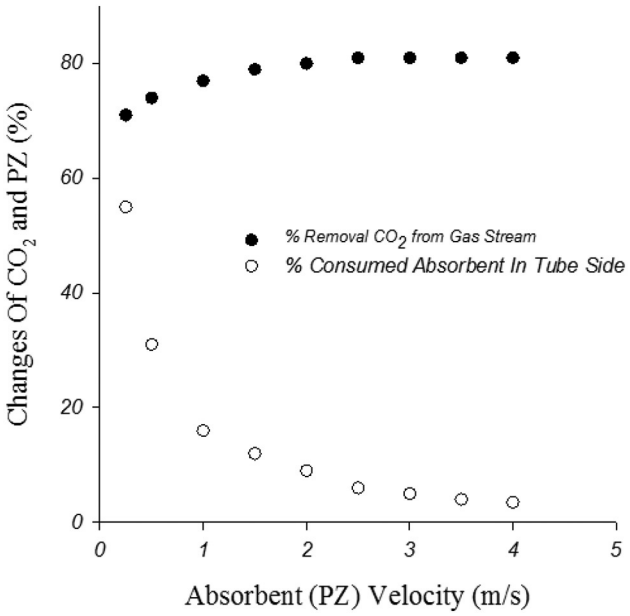


**Fig. 13.** Absorbent consumption at various absorbent velocities ($v_{gas}$ = 5 m/s, $C_{PZ}$ = 750 mol · m$^{-3}$).

in removing carbon dioxide from a gas mixture compared to the other absorbents.

2. Wettability is found to have a considerably negative impact on membrane carbon capture capacity. For instance, the modeling results show that even a 10% wetting of the membrane reduces the efficiency of the $CO_2$ removal process by more than 47%.
3. Modification of the membrane structure through adding nanoparticles to the membrane has a positive impact on system performance, so that adding 5% of MMT nanoparticles to membrane structure lead to 8% increase of carbon capture system efficiency.
4. System operating parameters including inlet gas flow rate to shell, inlet absorbent flow rate to tube and inlet absorbents concentration to tube are investigated. The results show that increasing the inlet gas velocity to the system has a negative impact on the system's performance in removing carbon dioxide particles. On the other hand, increasing the inlet absorbent speed as well as increasing the inlet absorbent concentration increases the efficiency of the system.
5. Increase in fiber packing density boosts the carbon capture efficiency in HFMC due to enhancing the residence time, contact area and subsequently better penetration of $CO_2$ into the membrane.
6. Absorbent consumption that is a disadvantage of such type of membrane separation systems can be minimized by adjusting the absorbent velocity below the absorbent velocity saturation limit (2 m/s in this work) where further increase in absorbent velocity would be associated with very limited increase in $CO_2$ removal.

## Symbols and notations

| | |
|---|---|
| $C_i$ | concentration of any species (mol · m$^{-3}$) |
| $C_{i-shell}$ | concentration of any species in the shell (mol · m$^{-3}$) |
| $C_{i-tube}$ | concentration of any species in the tube (mol · m$^{-3}$) |
| $C_{i-membrane}$ | concentration of any species in the membrane (mol · m$^{-3}$) |
| $C_{PZ}$ | initial PZ concentration in the liquid phase (mol · m$^{-3}$) |
| $C_{MEA}$ | initial MEA concentration in the liquid phase (mol · m$^{-3}$) |
| $C_{TEA}$ | Initial TEA concentration in the liquid phase (mol · m$^{-3}$) |
| $C_{EDA}$ | initial EDA concentration in the liquid phase (mol · m$^{-3}$) |
| $C_{in}$ | volumetric gas flow rate in the shell inlet (m$^3$ s$^{-1}$) |
| $C_{out}$ | volumetric gas flow rate in the shell outlet (m$^3$ s$^{-1}$) |
| $D_i$ | diffusion coefficient of any species (m$^2$ s$^{-1}$) |
| $D_{i-shell}$ | diffusion coefficient of any species in the shell (m$^2$ s$^{-1}$) |
| $D_{i-tube}$ | diffusion coefficient of any species in the tube (m$^2$ s$^{-1}$) |
| $D_{i-membrane}$ | diffusion coefficient of any species in the membrane (m$^2$ s$^{-1}$) |
| $D_{CO2,absorbent}$ | diffusivity of $CO_2$ in absorbent solution (m$^2$ s$^{-1}$) |
| $D_{N_2O,absorbent}$ | diffusivity of $N_2O$ in absorbent solution (m$^2$ s$^{-1}$) |
| $D_{CO_2,H2O}$ | diffusivity correlations of $CO_2$ in water (m$^2$ s$^{-1}$) |
| $D_{N_2O,H2O}$ | diffusivity correlations of $N_2O$ in water (m$^2$ s$^{-1}$) |
| $H$ | Henry's constant, KPad m$^3$ mol$^{-1}$ |
| $H_{N_2O,absorbent}$ | Henry's constant of $N_2O$ in absorbent solution (KPad m$^3$ mol$^{-1}$) |
| $H_{CO_2,H2O}$ | Henry's constant correlations of $CO_2$ in water (KPad m$^3$ mol$^{-1}$) |
| $H_{N_2O,H2O}$ | Henry's constant correlations of $N_2O$ in water (KPad m$^3$ mol$^{-1}$) |
| $J_i$ | diffusive flux of any species (mol m$^{-2}$ s$^{-1}$) |
| $L$ | length of the fiber (m) |
| $m_i$ | gas solubility in the absorbent liquid (mol mol$^{-1}$) |
| $Q_{in}$ | Gas flow rate at the inlet (m$^3$ s$^{-1}$) |
| $Q_{out}$ | Gas flow rate at the outlet (m$^3$ s$^{-1}$) |
| $r$ | radial coordinate (m) |
| $R_1$ | inner tube radius (m) |
| $R_2$ | outer tube radius (m) |
| $R_3$ | inner shell radius (m) |
| $R_i$ | reaction rate of any species (mol s$^{-1}$) |
| $R_w$ | Radius of wet part of membrane (m) |
| $S$ | total surface area of the membrane (m$^2$) |
| $T$ | temperature (K) |
| $T_g$ | temperature of the gas (K) |
| $u$ | average velocity in the shell side (m s$^{-1}$) |
| $v$ | average velocity in the tube side (m s$^{-1}$) |
| $V_z$ | axial velocity in the module (m s$^{-1}$) |
| $V_{z-shell}$ | axial velocity in the shell (m s$^{-1}$) |
| $V_{z-tube}$ | axial velocity in the tube (m s$^{-1}$) |
| $z$ | axial coordinate (m) |

*Greek letters*

| | |
|---|---|
| $\varphi$ | void volume inside the module |
| $\tau$ | tortuosity |
| $\varepsilon$ | porosity |
| $\mathbb{R}$ | module inner radius (m) |

## Author statement

- Hamed Abdolahi-Mansoorkhani: Conceptualization, Methodology, Writing, Modeling, Analyzing, Reviewing and editing
- Sadegh Seddighi: Idea, Conceptualization, Methodology, Analyzing, Writing, Modeling, Reviewing and editing, Supervision.

## Declaration of competing interest

The authors declare that they have no known competing financial interests or personal relationships that could have appeared to influence the work reported in this paper.

## Acknowledgment

This work is funded by Iran National Science Foundation (INSF) under the contract number 97007093.

## References

[1] Z. Dai, R.D. Noble, D.L. Gin, X. Zhang, L. Deng, Combination of ionic liquids with membrane technology: a new approach for $CO_2$ separation, J. Membr. Sci. 497 (2016) 1–20.
[2] S. Qazi, L. Gómez-Coma, J. Albo, S. Druon-Bocquet, A. Irabien, J. Sanchez-Marcano,

CO2 capture in a hollow fiber membrane contactor coupled with ionic liquid: influence of membrane wetting and process parameters, Sep. Purif. Technol. 233 (2020) 115986.
[3] B. Li, Y. Duan, D. Luebke, B. Morreale, Advances in CO2 capture technology: a patent review, Appl. Energy 102 (2013) 1439–1447.
[4] J. Haider, S. Saeed, M.A. Qyyum, B. Kazmi, R. Ahmad, A. Muhammad, M. Lee, Simultaneous capture of acid gases from natural gas adopting ionic liquids: challenges, recent developments, and prospects, Renew. Sust. Energ. Rev. 123 (2020) 109771.
[5] N. Sommerfeldt, H. Madani, In-depth techno-economic analysis of PV/Thermal plus ground source heat pump systems for multi-family houses in a heating dominated climate, Sol. Energy 190 (2019) 44–62.
[6] D.P. Hanak, V. Manovic, Linking renewables and fossil fuels with carbon capture via energy storage for a sustainable energy future, Front. Chem. Sci. Eng. (2019) 1–7.
[7] F. Johnsson, Perspectives on $CO_2$ capture and storage, Greenhouse Gases: Science and Technology 1 (2011) 119–133.
[8] M.B. Toftegaard, J. Brix, P.A. Jensen, P. Glarborg, A.D. Jensen, Oxy-fuel combustion of solid fuels, Prog. Energy Combust. Sci. 36 (2010) 581–625.
[9] S. Seddighi, P.T. Clough, E.J. Anthony, R.W. Hughes, P. Lu, Scale-up challenges and opportunities for carbon capture by oxy-fuel circulating fluidized beds, Appl. Energy 232 (2018) 527–542.
[10] S. Roussanaly, A. Aasen, R. Anantharaman, B. Danielsen, J. Jakobsen, L. Heme-De-Lacotte, G. Neji, A. Sødal, P.E. Wahl, T.K. Vrana, R. Dreux, Offshore power generation with carbon capture and storage to decarbonise mainland electricity and offshore oil and gas installations: a techno-economic analysis, Appl. Energy 233-234 (2019) 478–494.
[11] F. Massa, A. Coppola, F. Scala, A thermodynamic study of sorption-enhanced $CO_2$ methanation at low pressure, Journal of $CO_2$ Utilization 35 (2020) 176–184.
[12] X. Zhang, R. Zeng, K. Mu, X. Liu, X. Sun, H. Li, Exergetic and exergoeconomic evaluation of co-firing biomass gas with natural gas in CCHP system integrated with ground source heat pump, Energy Convers. Manag. 180 (2019) 622–640.
[13] W. Li, C. Lu, The multiple effectiveness of state natural gas consumption constraint policies for achieving sustainable development targets in China, Appl. Energy 235 (2019) 685–698.
[14] A. Jareteg, D. Maggiolo, S. Sasic, H. Ström, Finite-volume method for industrial-scale temperature-swing adsorption simulations, Comput. Chem. Eng. 106852 (2020).
[15] A. Almoslh, F. Alobaid, C. Heinze, B. Epple, Comparison of equilibrium-stage and rate-based models of a packed column for tar absorption using vegetable oil, Appl. Sci. 10 (2020) 2362.
[16] H. Wasajja, R.E. Lindeboom, J.B. van Lier, P. Aravind, Techno-economic review of biogas cleaning technologies for small scale off-grid solid oxide fuel cell applications, Fuel Process. Technol. 197 (2020) 106215.
[17] M. Biermann, H. Ali, M. Sundqvist, M. Larsson, F. Normann, F. Johnsson, Excess heat-driven carbon capture at an integrated steel mill – considerations for capture cost optimization, International Journal of Greenhouse Gas Control 91 (2019) 102833.
[18] Y. Han, W.W. Ho, Design of amine-containing $CO_2$-selective membrane process for carbon capture from flue gas, Ind. Eng. Chem. Res. 59 (12) (2019) 5340–5350.
[19] C.A. Scholes, Pilot plants of membrane technology in industry: challenges and key learnings, Front. Chem. Sci. Eng. (2019) 1–12.
[20] A. Iulianelli, E. Drioli, Membrane engineering: latest advancements in gas separation and pre-treatment processes, petrochemical industry and refinery, and future perspectives in emerging applications, Fuel Process. Technol. 206 (2020) 106464.
[21] A. Iulianelli, K. Ghasemzadeh, M. Marelli, C. Evangelisti, A supported Pd-Cu/$Al_2O_3$ membrane from solvated metal atoms for hydrogen separation/purification, Fuel Process. Technol. 195 (2019) 106141.
[22] S. Dong, Z. Wang, M. Sheng, Z. Qiao, J. Wang, High-performance multi-layer composite membrane with enhanced interlayer compatibility and surface cross-linking for $CO_2$ separation, J. Membr. Sci. 118221 (2020).
[23] R. Zeynali, K. Ghasemzadeh, A. Iulianelli, A. Basile, Experimental evaluation of graphene oxide/$TiO_2$-alumina nanocomposite membranes performance for hydrogen separation, Int. J. Hydrog. Energy 45 (2020) 7479–7487.
[24] A. Iulianelli, A. Basile, Hybrid and inorganic membranes for $CO_2$/$H_2$ separation process, Current Trends and Future Developments on (Bio-) Membranes, Elsevier, 2018, pp. 289–305.
[25] P. Bernardo, E. Drioli, G. Golemme, Membrane gas separation: a review/state of the art, Ind. Eng. Chem. Res. 48 (2009) 4638–4663.
[26] U.W. Siagian, A. Raksajati, N.F. Himma, K. Khoiruddin, I.G. Wenten, Membrane-based carbon capture technologies: membrane gas separation vs. membrane contactor, Journal of Natural Gas Science and Engineering 67 (2019) 172–195.
[27] K. He, L.-Z. Zhang, Fluid flow and heat transfer of cross flow hollow fiber membrane contactors with randomly distributed fibers: a topological study, Int. J. Heat Mass Transf. 135 (2019) 186–198.
[28] R. Wang, D. Li, D. Liang, Modeling of $CO_2$ capture by three typical amine solutions in hollow fiber membrane contactors, Chem. Eng. Process. Process Intensif. 43 (2004) 849–856.
[29] F. Zhou, H.N. Tien, Q. Dong, W.L. Xu, H. Li, S. Li, M. Yu, Ultrathin, ethylenediamine-functionalized graphene oxide membranes on hollow fibers for $CO_2$ capture, J. Membr. Sci. 573 (2019) 184–191.
[30] A. Köhler, D. Pallarès, F. Johnsson, Modeling axial mixing of fuel particles in the dense region of a fluidized bed, Energy Fuel 34 (2020) 3294–3304.
[31] J.-L. Li, B.-H. Chen, Review of $CO_2$ absorption using chemical solvents in hollow fiber membrane contactors, Sep. Purif. Technol. 41 (2005) 109–122.
[32] O.G. Nik, X.Y. Chen, S. Kaliaguine, Functionalized metal organic framework-polyimide mixed matrix membranes for $CO_2$/$CH_4$ separation, J. Membr. Sci. 413 (2012) 48–61.
[33] S. Hwang, W.S. Chi, S.J. Lee, S.H. Im, J.H. Kim, J. Kim, Hollow ZIF-8 nanoparticles improve the permeability of mixed matrix membranes for CO2/CH4 gas separation, J. Membr. Sci. 480 (2015) 11–19.
[34] M.H. El-Naas, M. Al-Marzouqi, S.A. Marzouk, N. Abdullatif, Evaluation of the removal of $CO_2$ using membrane contactors: membrane wettability, J. Membr. Sci. 350 (2010) 410–416.
[35] H.-Y. Zhang, R. Wang, D.T. Liang, J.H. Tay, Theoretical and experimental studies of membrane wetting in the membrane gas–liquid contacting process for $CO_2$ absorption, J. Membr. Sci. 308 (2008) 162–170.
[36] M.H. Ibrahim, M.H. El-Naas, Z. Zhang, B. Van der Bruggen, $CO_2$ capture using hollow fiber membranes: a review of membrane wetting, Energy Fuel 32 (2018) 963–978.
[37] S.-H. Yeon, B. Sea, Y.-I. Park, K.-H. Lee, Determination of mass transfer rates in PVDF and PTFE hollow fiber membranes for $CO_2$ absorption, Sep. Sci. Technol. 38 (2003) 271–293.
[38] Y. Xu, Y. Lin, N.G.P. Chew, C. Malde, R. Wang, Biocatalytic PVDF composite hollow fiber membranes for $CO_2$ removal in gas-liquid membrane contactor, J. Membr. Sci. 572 (2019) 532–544.
[39] J. Franco, D. Demontigny, S. Kentish, J. Perera, G. Stevens, A study of the mass transfer of $CO_2$ through different membrane materials in the membrane gas absorption process, Sep. Sci. Technol. 43 (2008) 225–244.
[40] K. Ghasemzadeh, J.N. Harasi, T.Y. Amiri, A. Basile, A. Iulianelli, Methanol steam reforming for hydrogen generation: a comparative modeling study between silica and Pd-based membrane reactors by CFD method, Fuel Process. Technol. 199 (2020) 106273.
[41] S.-H. Lin, K.-L. Tung, W.-J. Chen, H.-W. Chang, Absorption of carbon dioxide by mixed piperazine–alkanolamine absorbent in a plasma-modified polypropylene hollow fiber contactor, J. Membr. Sci. 333 (2009) 30–37.
[42] A. Rosli, A.L. Ahmad, S.C. Low, Anti-wetting polyvinylidene fluoride membrane incorporated with hydrophobic polyethylene-functionalized-silica to improve $CO_2$ removal in membrane gas absorption, Sep. Purif. Technol. 221 (2019) 275–285.
[43] M. Fosi-Kofal, A. Mustafa, A. Ismail, M. Rezaei-DashtArzhandi, T. Matsuura, PVDF/$CaCO_3$ composite hollow fiber membrane for CO2 absorption in gas–liquid membrane contactor, Journal of Natural Gas Science and Engineering 31 (2016) 428–436.
[44] P. Kumar, J. Hogendoorn, P. Feron, G. Versteeg, New absorption liquids for the removal of $CO_2$ from dilute gas streams using membrane contactors, Chem. Eng. Sci. 57 (2002) 1639–1651.
[45] M. Al-Marzouqi, M. El-Naas, S. Marzouk, N. Abdullatif, Modeling of chemical absorption of $CO_2$ in membrane contactors, Sep. Purif. Technol. 62 (2008) 499–506.
[46] K. Simons, K. Nijmeijer, M. Wessling, Gas–liquid membrane contactors for $CO_2$ removal, J. Membr. Sci. 340 (2009) 214–220.
[47] M. Saidi, $CO_2$ absorption intensification using novel DEAB amine-based nanofluids of CNT and $SiO_2$ in membrane contactor, Chemical Engineering and Processing-Process Intensification 107848 (2020).
[48] H. Li, Z. Zhang, Mining the intrinsic trends of $CO_2$ solubility in blended solutions, Journal of $CO_2$ Utilization 26 (2018) 496–502.
[49] M.R. DashtArzhandi, A. Ismail, T. Matsuura, Carbon dioxide stripping through water by porous PVDF/montmorillonite hollow fiber mixed matrix membranes in a membrane contactor, RSC Adv. 5 (2015) 21916–21924.
[50] A. Hosseinzadeh, M. Hosseinzadeh, A. Vatani, T. Mohammadi, Mathematical modeling for the simultaneous absorption of $CO_2$ and $SO_2$ using MEA in hollow fiber membrane contactors, Chem. Eng. Process. Process Intensif. 111 (2017) 35–45.
[51] R.B. Bird, Transport phenomena, Appl. Mech. Rev. 55 (2002) R1–R4.
[52] J. Happel, Viscous flow relative to arrays of cylinders, AICHE J. 5 (1959) 174–177.
[53] R. Faiz, M. Al-Marzouqi, Mathematical modeling for the simultaneous absorption of $CO_2$ and $H_2S$ using MEA in hollow fiber membrane contactors, J. Membr. Sci. 342 (2009) 269–278.
[54] M. Mehdipourghazi, S. Barati, F. Varaminian, Mathematical modeling and simulation of carbon dioxide stripping from water using hollow fiber membrane contactors, Chem. Eng. Process. Process Intensif. 95 (2015) 159–164.
[55] R.B. Bird, W.E. Stewart, E.N. Lightfoot, Transport Phenomena, John Wiley & Sons, New York, 1960, p. 413.
[56] G.F. Versteeg, W. Van Swaalj, Solubility and diffusivity of acid gases (carbon dioxide, nitrous oxide) in aqueous alkanolamine solutions, Journal of Chemical and Engineering Data 33 (1988) 29–34.
[57] H. Abdolahi-Mansoorkhani, S. Seddighi, $H_2S$ and $CO_2$ capture from gaseous fuels using nanoparticle membrane, Energy 168 (2019) 847–857.
[58] A.P. Salvi, P.D. Vaidya, E.Y. Kenig, Kinetics of carbon dioxide removal by ethylenediamine and diethylenetriamine in aqueous solutions, Can. J. Chem. Eng. 92 (2014) 2021–2028.
[59] W.-C. Sun, C.-B. Yong, M.-H. Li, Kinetics of the absorption of carbon dioxide into mixed aqueous solutions of 2-amino-2-methyl-l-propanol and piperazine, Chem. Eng. Sci. 60 (2005) 503–516.
[60] D. Barth, C. Tondre, J.J. Delpuech, Stopped-flow investigations of the reaction kinetics of carbon dioxide with some primary and secondary alkanolamines in aqueous solutions, Int. J. Chem. Kinet. 18 (1986) 445–457.
[61] S.-W. Park, B.-S. Choi, J.-W. Lee, Chemical absorption of carbon dioxide with triethanolamine in non-aqueous solutions, Korean J. Chem. Eng. 23 (2006) 138–143.
[62] W.M. Haynes, CRC Handbook of Chemistry and Physics, CRC Press, 2014.
[63] M.J. O'Neil, A. Smith, P.E. Heckelman, S. Budavari, The Merck Index-An Encyclopedia of Chemicals, Drugs, and Biologicals, vol. 767, Merck and Co, Inc., Whitehouse Station, NJ, 2001, p. 4342.

[64] N.C.f.B.I.P. Database, Ethylenediamine, CID = 3301, https://pubchem.ncbi.nlm.nih.gov/compound/Ethylenediamine.
[65] M. Williams, M.J. O'Neil (Ed.), The Merck Index: An Encyclopedia of Chemicals, Drugs, and Biologicals, Royal Society of Chemistry, Cambridge, UK, 9781849736701, April 2013(2708 pages, $150 with 1-year free access to The Merck Index Online, in, 2013).
[66] S. Budavari, M. O'neil, A. Smith, P. Heckelman, J. Obenchain Jr., J. Gallipeau, M. D'Arecea, The Merck Index: An Encyclopedia of Chemicals, Drugs, and Biologicals, vol. 450, Merck & Co, Inc., Whitehouse Station, NJ, 1996, p. 1674.
[67] N.T. Program, Institute of Environmental Health Sciences, National Institutes of Health (NTP), National Toxicology Program Chemical Repository Database, NTP, Research Triangle Park, North Carolina, 1992 via http://canieochemicals.noaa.gov/chemical/20568.
[68] A. Muhammad, M.I.A. Mutalib, T. Murugesan, A. Shafeeq, Thermophysical properties of aqueous piperazine and aqueous (N-methyldiethanolamine + piperazine) solutions at temperatures (298.15 to 338.15) K, J. Chem. Eng. Data 54 (2009) 2317–2321.
[69] G. Vázquez, E. Alvarez, R. Rendo, E. Romero, J.M. Navaza, Surface tension of aqueous solutions of diethanolamine and triethanolamine from 25 °C to 50 °C, J. Chem. Eng. Data 41 (1996) 806–808.
[70] L. Zhao, Q. Li, L. Ma, C. Liu, F. Sha, J. Zhang, Liquid density, viscosity, surface tension, and spectroscopic investigation of 1, 2-ethanediamine + 1, 2-propanediol for $CO_2$ capture, J. Mol. Liq. 241 (2017) 374–385.
[71] E.L. Cussler, E.L. Cussler, Diffusion: Mass Transfer in Fluid Systems, Cambridge University Press, 2009.
[72] S. Paul, A.K. Ghoshal, B. Mandal, Removal of $CO_2$ by single and blended aqueous alkanolamine solvents in hollow-fiber membrane contactor: modeling and simulation, Ind. Eng. Chem. Res. 46 (2007) 2576–2588.
[73] A.T. Nakhjiri, A. Heydarinasab, O. Bakhtiari, T. Mohammadi, The effect of membrane pores wettability on $CO_2$ removal from $CO_2/CH_4$ gaseous mixture using NaOH, MEA and TEA liquid absorbents in hollow fiber membrane contactor, Chinese Journal of Chemical Engineering 26 (2018) 1845–1861.
[74] S. Bishnoi, G.T. Rochelle, Absorption of carbon dioxide into aqueous piperazine: reaction kinetics, mass transfer and solubility, Chem. Eng. Sci. 55 (2000) 5531–5543.
[75] S. Zhou, X. Chen, T. Nguyen, A.K. Voice, G.T. Rochelle, Aqueous ethylenediamine for $CO_2$ capture, ChemSusChem 3 (2010) 913–918.
[76] S. Atchariyawut, R. Jiraratananon, R. Wang, Separation of $CO_2$ from $CH_4$ by using gas–liquid membrane contacting process, J. Membr. Sci. 304 (2007) 163–172.
[77] S.-H. Yeon, K.-S. Lee, B. Sea, Y.-I. Park, K.-H. Lee, Application of pilot-scale membrane contactor hybrid system for removal of carbon dioxide from flue gas, J. Membr. Sci. 257 (2005) 156–160.
[78] L. Pisani, Simple expression for the tortuosity of porous media, Transp. Porous Media 88 (2011) 193–203.
[79] M. Mesbah, M. Jafari, E. Soroush, S. Shahsavari, Mathematical modeling and numerical simulation of $CO_2$ removal by using hollow fiber membrane contactors, Iranian Journal of Oil & Gas Science and Technology 6 (2017) 80–96.
[80] S.-p. Yan, M.-X. Fang, W.-F. Zhang, S.-Y. Wang, Z.-K. Xu, Z.-Y. Luo, K.-F. Cen, Experimental study on the separation of $CO_2$ from flue gas using hollow fiber membrane contactors without wetting, Fuel Process. Technol. 88 (2007) 501–511.
[81] M. Niknam, P. Zare, P. Keshavarz, Experimental and modeling study of $CO_2$ absorption by L-Proline promoted potassium carbonate using hollow fiber membrane contactor, International Journal of Greenhouse Gas Control 93 (2020) 102877.
[82] M. Mesbah, M. Momeni, E. Soroush, S. Shahsavari, S.A. Galledari, Theoretical study of $CO_2$ separation from $CO_2/CH_4$ gaseous mixture using 2-methylpiperazine-promoted potassium carbonate through hollow fiber membrane contactor, Journal of Environmental Chemical Engineering 7 (2019) 102781.
[83] Z. Dai, M. Usman, M. Hillestad, L. Deng, Modelling of a tubular membrane contactor for pre-combustion $CO_2$ capture using ionic liquids: influence of the membrane configuration, absorbent properties and operation parameters, Green Energy & Environment 1 (2016) 266–275.